Detecting Depth of Desiccation-Induced Clay Crack Based on Anisotropy Index (AI) of Apparent Electrical Resistivity

Haoze Wu[1, 2], Chungfai Chiu[1, 2*]

[1]*Department of Civil and Environmental Engineering, Shantou University, Shantou, Guangdong, China*

[2]*Guangdong Structural Safety and Monitoring Engineering Technology Research Centre, Shantou, Guangdong, China*

**Corresponding Author.*

Abstract

As the global climate warms, the soil is much easier to crack. In order to study the method of detecting the soil crack depth, a desiccation soil crack experiment was performed indoors. First, the soil-water characteristic curve (SWCC) of kaolin was measured by the filter paper method. During the desiccation process, the variation process of suction and volumetric water content was studied. For soil surface cracks, the propagation process of cracks was measured using a camera. Anisotropy index (AI) of apparent electrical resistivity was measured by a multi-layer electrode array. Based on the electrical resistivity method (ERM) and a numerical simulation of a multi-layer electrode array for a single crack, a new method to detect the crack depth was proposed. This method was used to predict the depth of cracks during the desiccation experiment, and the results were compared to crack depths obtained using the crack-tip opening angle (CTOA) method. The results show that this method is simpler and can detect the soil crack depth well. This research provides a method to detect the crack depth, which can be used to monitor the crack depth in some soil structures, such as landfill cover and dams.

Keywords: *Desiccation crack depth, Electrical resistivity method, Anisotropy index, Crack-tip opening angle*

I. Introduction

Due to the impact of global warming, the desiccation caused by the extreme climate is one of the most important factors that make the soil crack. Cracks are common in clayey and expansive soils in many construction sites and irrigated areas [1]. Some studies have already shown that cracks have significant impacts on the mechanical and hydraulic properties of soil [2, 3]. In general, soil cracks could cause various geotechnical and environmental issues, such as landslides and mudflow [4], creating preferential flow paths for rainfalls and contaminants in landfill covers and liners [5, 6], and reducing the stability and performance of earth infrastructures [7]. Wang et al. [8] compared cracked soil with intact soil and found that the hydraulic conductivity of the former was several orders of magnitude higher than that of the latter. Therefore, the soil structures of low permeability need to prevent cracking and conduct crack monitoring. In liners and covers of landfill and nuclear waste isolation, the crack depth has the greatest influence on the sealing performance [9], so detecting crack depth is very important.

In recent years, many different approaches have been proposed to map and quantify soil crack geometry characteristics [10], while the effective approaches in situ detection of crack dynamics are still difficult to be found up to now. The quantification of cracks on the soil surface was often manually observed and recorded in the past [11]. Because the measurement results depend on the subjectivity of observers, those often have large errors. In order to avoid errors caused by manual measurement, image analysis techniques are currently used for soil surface cracks. Image analysis technology has proven to be a useful tool, which can be used to determine the geometric characteristics of the crack width, length, area, etc. more accurately [12]. However, due to the influence of the surface vegetation, it is difficult to monitor the cracks on the soil surface with observation and image analysis

techniques [7]. Moreover, some cracks propagate within the soil and develop upwards, so the cracks are often not detected in real time.

Compared with the detection of soil surface cracks, the detection of crack depth is more important and more difficult. The crack depth is an important factor in determining the damage of the soil structure, such as landfill cover and dams. The detection methods of soil crack depth can be classified into two groups: destructive and non-destructive techniques. Serial sectioning of soil [13], digging soil trenches [14], pushing a probe wire into the crack [15] and pouring liquid latex [16], etc. are the destructive techniques. These methods cannot detect the crack depth in real time, and may also destroy the original crack pattern in the measurement process. The non-destructive techniques can solve these problems, such as ground penetration radar (GPR) [17], non-contact laser scanner system [18] and electrical resistivity method (ERM) [19, 20]. In recent years, non-destructive technology has become an attractive method for detecting desiccation cracks in soil. In particular, the resistivity method has good application prospects in the detection of soil crack propagation.

The quantitative studies of geometric characteristics of soil cracks have extremely important practical implications, especially in detecting the crack depth. Samouëlian et al. [21] used the anisotropy index (AI) of apparent electrical resistivity as the detection index to detect the cracks. Greve et al. [22] combined electrical resistivity tomography (ERT) technology to further explain AI changes with water content and cracks. Hassan et al. [23] demonstrated that AI provides a way to detect subsurface through resistivity measurement. Qin et al. [24] studied the relationship between AI and vertical strain during compression of compacted loess. As an index, the applicability of using AI to detect the crack depth or crack propagation area needs to be studied. The objective of this paper is to detect the crack depth in clay using the electrical resistivity method which is achieved by anisotropy index (AI) of apparent electrical resistivity. This paper establishes a non-destructive and real-time detection method of soil crack depth, which can detect the crack depth quickly and accurately, and it is less affected by external interference during the detection process.

II. Materials and Method

2.1 Soil

In this study, we aim to detect the crack depth of clay soil. Kaolin clay has typically been used as the landfill cover soil. Pure kaolin was used in this experiment. Its specific gravity, liquid limit, plastic limit and maximum dry density are 2.69, 55.2%, 30.3% and 1.28 Mg/m^3, respectively. The particle size distribution curve of the studied kaolin reveals that the silt content is 23% and the clay content is 77% (Fig. 1). According to the Unified Soil Classification System (USCS), the soil is classified as highly plastic clay (CH).

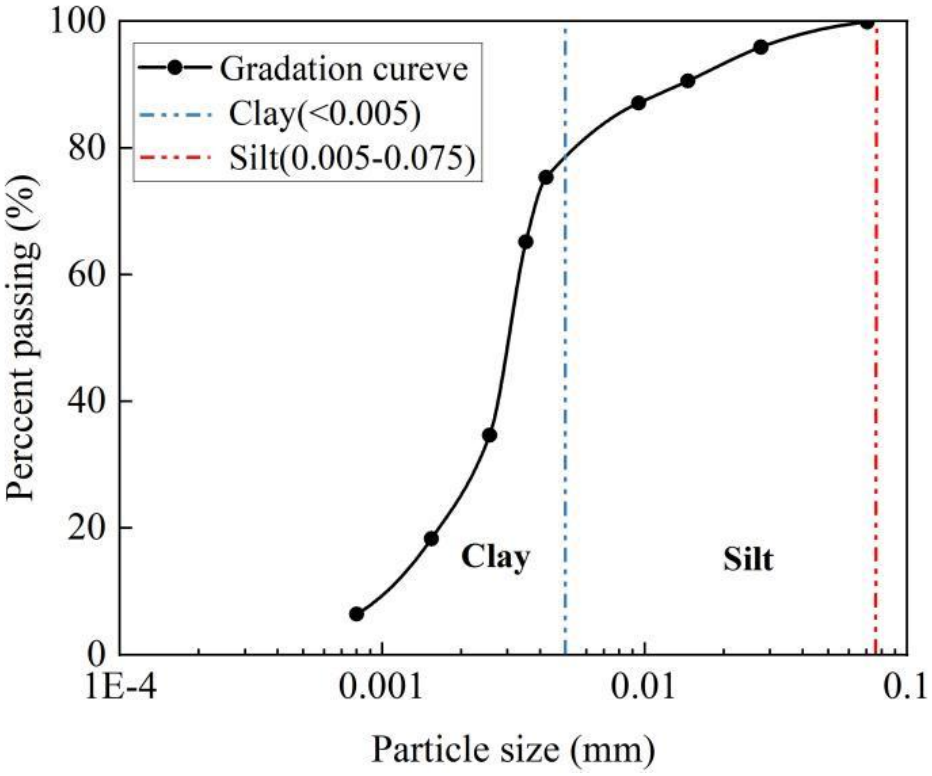

Fig 1: Particle size distribution curve of the studied kaolin

2.2 Filter paper method

The soil-water characteristic curve (SWCC) is determined by the basic properties of the soil, and it is important for the study of unsaturated soils. The filter paper method has a larger test range, and it is cheaper and simpler to use than the tensiometer method and centrifuge method. In this study, we used the filter paper method to measure the SWCC of the kaolin. The principle of the filter paper method is that the water in the soil is absorbed by the dry filter paper to reach suction equilibrium, and the matrix suction of the soil is determined from the water content of the filter paper at suction equilibrium [25]. The common filter paper is the Whatman No.42, and we used it to get SWCC. The procedure for the filter paper method and Whatman's rate curve can be found in ASTM. The calibration functions are shown below (ASTM D5298-10 2013):

$$\lg\psi = \begin{cases} 5.32 - 0.07 w_{fp}, w_{fp} < \\ 2.412 - 0.0135 w_{fp}, w_{fp} \geq 45.3\% \end{cases} \quad (1)$$

Where ψ (kPa) is soil matric suction, and w_{fp} is the gravimetric water content of filter paper.

2.3 Electrical resistivity method

The apparent electrical resistivity is a material parameter of soil, and the unit is Ω·m. There are two methods for measuring the apparent electrical resistivity of soil, including the two-electrode method and the four-electrode method. Although the two-electrode method is relatively simple, it is susceptible to the influence of contact resistance, which leads to larger data errors than four-electrode method. Therefore, the four-electrode method was used to measure the apparent electrical resistivity in this experiment. The current I (A) is injected into the soil through two electrodes C1 and C2 (Fig. 2), and the resulting potential difference ΔU (V) is measured by the other two electrodes P1 and P2 (Fig. 2). Anisotropy index (AI) was first proposed by Samouëlian et al. to study the anisotropy degree of soil [21], which is based on square arrays to characterize the influence of soil cracks on soil anisotropy. Resistivity ρ and AI are calculated by the following equations:

$$\rho = K\frac{\Delta U}{I} \tag{2}$$

$$\mathrm{AI} = \frac{\rho_\alpha}{\rho_\beta} \tag{3}$$

where K is the geometric coefficient that considers the correlation between the current flow within the material and the geometry of the electrodes, as well as the arrangement of electrodes. The ρ_α and ρ_β indicate the apparent electrical resistivity of α array and β array [22]. The configurations of α array and β array are shown in Fig. 2.

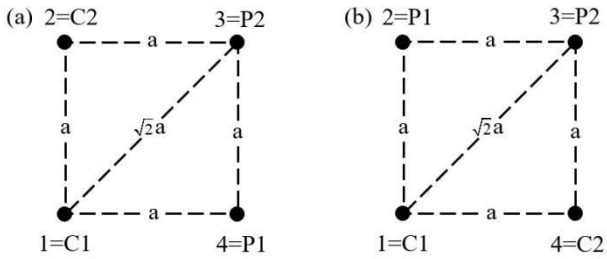

Fig 2: Plan view of a square array: (a) α array, (b) β array

2.4 Desiccation cracks experiment and measuring resistivity

The soil model size is 400 mm long, 400 mm wide, and 440 mm deep in a chamber. The bottom of the chamber was filled with a 40 mm sand cushion, and then the kaolin was evenly filled into the chamber with a dry density of 1.2 Mg/m3. In order to collect the distribution of suction and volumetric water content in the soil during the desiccation, four high capacity tensiometers (HCT) were installed, and their burial depths are 15 mm, 60 mm, 120 mm and 180 mm, respectively. The four EC-5 moisture sensors were symmetrically arranged at the same buried depth as HCT. These sensors were about 50 mm away from the boundary of the chamber to reduce the boundary effect in the process of soil desiccation shrinkage.

Twelve copper sheet electrodes were fixed to a cylindrical plexiglass tube with a diameter of 15 mm at 30 mm intervals. Wires and a tube with electrodes make up the electrode string. A square area with a side length of 200 mm was marked on the soil surface, and then it was divided into four same squares. Nine electrode strings were installed at nine vertices of square region, which was divided into four cells (I, II, III, IV) in Fig.3. During the experiment, the electrical resistivity of the crack soil was measured by twelve electrode layers. In order to clarify the direction of surface cracks, the coordinate system was established to describe the propagation direction of surface cracks in Fig. 3.

In order to reduce the influence of dry-wet cycles on soil cracks, we added about 100 mm of water above the soil to make the soil saturated before the desiccation [26]. A fan was placed above the model to accelerate the evaporation process and to make the evaporation relatively homogeneous after the soil was saturated [27]. The soil was at a constant temperature and humidity environment. The temperature was about 20℃, and the humidity was about 80%. Due to the low temperature and high humidity, we predicted that the soil would be difficult to crack [28]. Therefore, a high-temperature sodium lamp was used for local heating above cell III to promote local evaporation rate. During the desiccation process, it was heated six times and for one and a half hours each time. During the laboratory desiccation experiment, a camera was fixed above the chamber to take pictures of the soil surface at different desiccation times. The camera used in this study is the Cannon A640 optical camera, and this camera can be controlled by the program and stored in the computer synchronously.

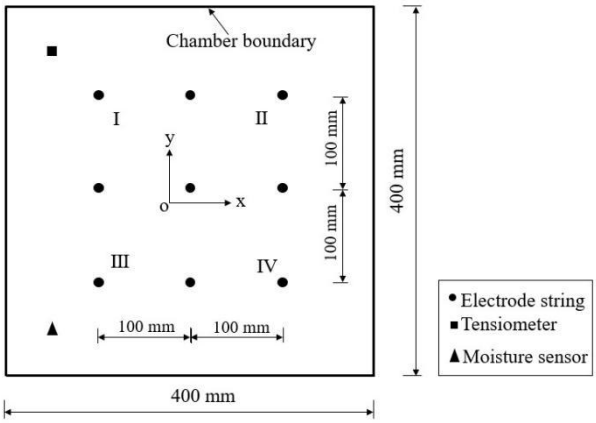

Fig 3: Top view of the arrangement of electrode strings, the tensiometers and moisture sensors.

2.5 Numerical Simulation of a multi-layer electrode array

In order to verify the hypothesis of measuring crack depth based on AI, we established a numerical model of a multilayer electrode array based on the finite element method. The side length of the square electrode array is a, and the distance between the electrode arrays of different layers is 0.1a. In this study, a total of 21 layers of electrodes are set. The simulated crack depths are 0.6a, 0.7a, 0.9a, 1.0a, 1.6a, 1.7a, 1.8a and 1.9a, respectively. The resistivities obtained by numerical simulation are further calculated to get AI by Equation (3). The frequency of the alternating current is 50 Hz (Chinese civil power frequency). In this case, the electric field was assumed to be a quasi-static electric field, so Poisson equation is used to describe the electrical field. The Poisson equation [29] is as follows:

$$\nabla^2 U = -\rho_0 / \varepsilon_0 \tag{4}$$

Where U is the electric potential, ρ_0 is charge density, and ε_0 is permittivity.

The setting of boundary conditions is one of the most important steps in the numerical simulation calculation. This study established the soil in a limited area. It is assumed that the boundary condition of the study area is the insulating boundary in an ideal state [30], and it is shown as follows:

$$\partial U / \partial n = 0 , \text{ on } \Gamma \tag{5}$$

The geometry of the crack part also needs to be given material and boundary conditions. In the case of actual current conduction, it can be considered that the crack part is an insulator, and the current needs to flow around the boundary conditions. Therefore, it can be assumed that the crack is non-conductive, which satisfies Equation (5).

2.6 The method of crack-tip opening angle

Previous studies showed that crack-tip opening angle (CTOA) was a special property of material failure, and it was assumed to remain unchanged at the desiccation process [31]. Therefore, when the maximum crack width on the soil surface is known, the CTOA could be used to estimate the maximum crack depth. The maximum cracking width (w) was measured using a vernier caliper for each cell, and the widest place was excavated at the same time to measure the depth of crack (h) after the experiment. According to the maximum crack width and depth, the CTOA can be calculated according to Equation (6):

$$\text{CTOA} = 2\arctan\left(w / 2h\right) \tag{6}$$

III. Results and Discussions

3.1 SWCC of kaolin

At present, based on the test data of matrix suction and water content, some soil-water characteristic curve fitting models are used for parameter fitting. The VG model is commonly used, and its expression is shown in the following equation [32].

$$\theta_w = \theta_r + \frac{\theta_s - \theta_r}{[1+(\alpha \cdot \psi)^n]^m} \quad (7)$$

Where θ_w is the volumetric water content; θ_s is the saturated water content; θ_r is the residual water content; ψ is the matric suction; α, n and m are the curve parameters; m = 1-1/n.

This study used the contact filter paper method to determine the SWCC of kaolin [33]. This method directly contacts and seals the test filter paper with the soil sample. Under relatively constant temperature and humidity conditions, the water in the soil sample migrates to the dry filter paper in the form of liquid water flow. When the suction of the filter paper is equal to the suction of the soil sample, the matrix suction of the soil sample is indirectly determined by the corresponding relationship between the water content of the filter paper and the suction (Equation 1). The experimental results of the filter paper method are shown in the Fig. 4. The horizontal axis is the matrix suction, the vertical axis is the volumetric water content, the black squares are the experimental data points of kaolin SWCC, and the red line is the VG fitting curve. It can be seen that the distribution of test points fits well with the VG fitting curve. The fitting parameters are θ_s = 57.70%, θ_r = 13.39%, α = 0.00567, n = 1.68, respectively. According to the SWCC, the air entry value of this kaolin is about 100 kPa.

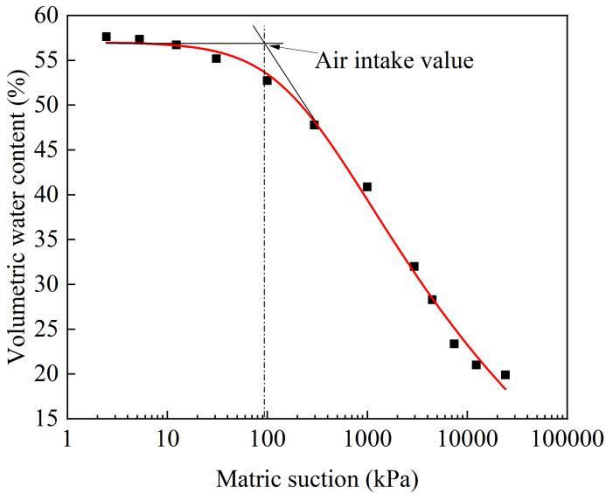

Fig 4: Soil-water characteristic curve of kaolin

3.2 The variations of suction and water content in soil

The desiccation process lasted for 18 days, and the suctions at different depths in the soil are shown in Fig. 5a. The suctions at different depths changed very slightly during the desiccation process. The moisture contents measured at different depths in the soil are shown in Fig. 5b. During the 18 days desiccation process, the moisture content only changed by about 3%. The reason for this phenomenon may be that the laboratory temperature is low, the humidity is high, the total suction is low, and the water loss of soil is relatively difficult. The soil sample can be considered saturated all the time, because the air intake value of the kaolin is about 100 kPa, which means that the kaolin sample is saturated if it is lower than it [34]. According to Fig. 4, the water contents corresponding to the suction of 15 mm and 60 mm burial depth are greater than the water content actually measured in Fig. 5b. This may be because there are cracks on the surface and inside of the soil, making the soil produce a greater change in water content than the non-fractured soil within the same suction change range [35]. After the experiment, 10 points were taken on the soil surface to measure the volumetric moisture content. The volumetric water content on the soil surface of cell Ⅰ and cell Ⅲ was about 40% to 44%. The volumetric water content on the surface of cell Ⅱ cell Ⅳ was approximately 48%.

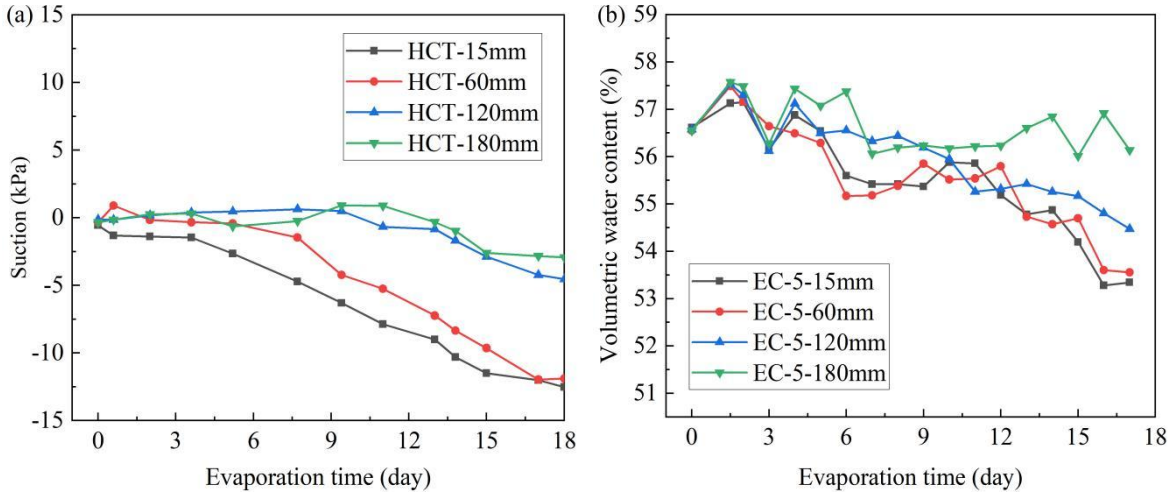

Fig 5: (a) The change of suction; (b) The change of volumetric water content in different depth of soil

3.3 The propagation of surface cracks

Due to the inhomogeneous distribution of water content on the soil surface during desiccation, the parts of the soil with a low water content shrink more than the parts in the soil with a relatively higher water content [36]. As a result, some cracks of the soil surface can be seen in Fig. 6, and the cracks are greater in cell Ⅰ and cell Ⅲ with lower water content. During the desiccation process of the soil sample, the change of surface cracks can be recorded by the camera to analyze the propagation of soil surface cracks. The pictures of the soil surface that has just been desiccated and the soil surface that has been desiccated for 17.3 days are shown in Fig. 6. Because the soil sample is uniform and saturated for a long time, there are no cracks in Fig 6 a. After 17.3 days of desiccation, many cracks have appeared on the soil surface (Fig. 6b). The cell Ⅰ and cell Ⅲ both have a crack with the largest width and the longest length, which can be called primary cracks. The other cracks are called the secondary cracks because they are shorter and narrower [20].

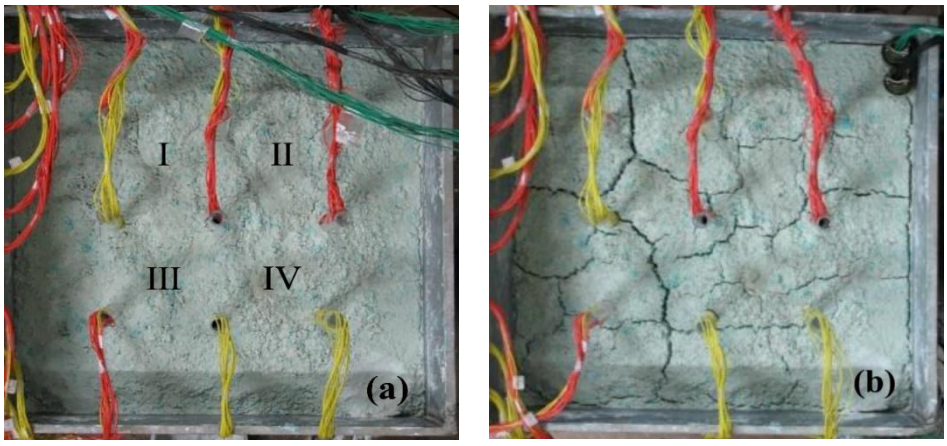

Fig 6: (a) Soil surface desiccated cracks at 0 day, (b) Soil surface cracks at 17.3 day

It can be seen from the pictures of soil surface cracks that the width of cracks in cell III is the widest, and the number of cracks is the largest among the four cells due to the placement of the sodium lamp above unit III for heating. It is easy to distinguish between primary cracks and secondary cracks in unit I and unit III. For the study of surface crack morphology, previous studies have shown that cracks mainly intersect at 90 ° and 120 ° [36] and this rule can be clearly obtained from Fig. 6. Wang et al. [37] analyzed the stress field based on digital image correlation technology. The result showed that desiccation cracks belong to mode Ⅰ, and the surrounding stress

is redistributed, causing adjacent cracks to intersect orthogonally. Measuring the width of the crack, and then the CTOA method can be used to analyze the depth of cracks at different times during soil desiccation. During the desiccation process, we measure the maximum crack width of each cell at different times to provide width data for the subsequent prediction of the crack depth using the CTOA method. The maximum cracks width of each cell at different desiccation times are provided in Table 1.

Table 1 Maximum widths of four cell cracks in different drying times

Desiccation time	Maximum crack width (mm)			
(d)	Ⅰ cell	Ⅱ cell	Ⅲ cell	Ⅳ cell
3.1	1.16	0.67	1.16	1.16
6.0	2.12	1.73	2.12	1.64
9.9	3.47	1.93	3.78	1.87
13.3	4.81	3.37	5.30	2.79
17.3	5.78	3.95	6.44	3.10

3.4 The measurement of AI during desiccation

This study focused on the variations of anisotropy indexes (AIs) distributed along the burial depth during the desiccation and proposed a method to detect the crack depth according to it. Therefore, the AIs of apparent electrical resistivity were measured at different times in the experiment. During the eighteen-day evaporation process, the distributions of AI along the electrodes burial depth in four cells were tested on day 3.1, day 6.0, day 9.9, day 13.3, and day 17.3, respectively. The surface crack widths of the cell Ⅰ and cell Ⅲ are larger than those of the cell Ⅱ and cell Ⅳ, so the cracks of the cell Ⅰ and cell Ⅲ propagate more completely. Taking the cell Ⅰ and cell Ⅲ as an example, the AIs of the two cells are shown in Fig. 7.

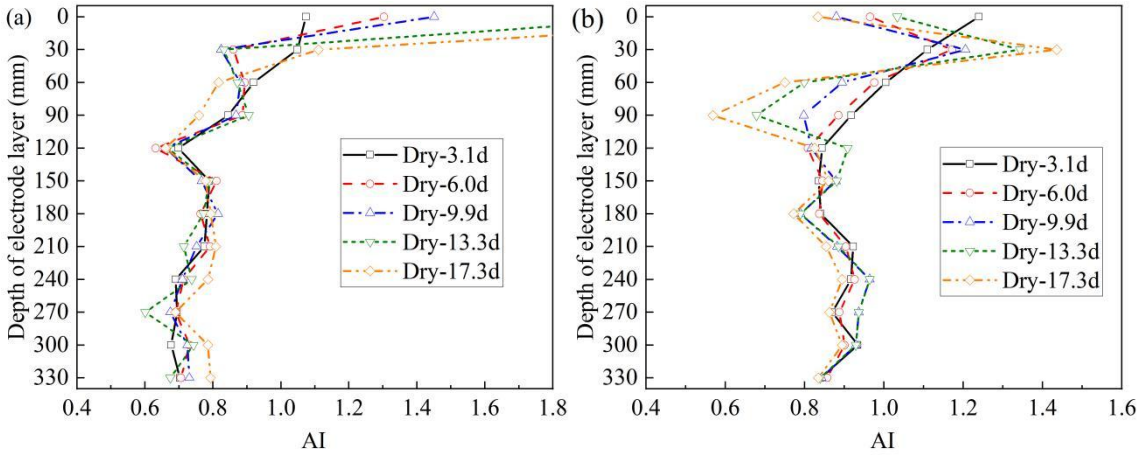

Fig 7: AIs at different depths during desiccation: (a) cell I, (b) cell III

There are some irregular points of test data in Fig. 7, which may be caused by manual measurement errors. Most of the AIs corresponding to the burial depth of the electrode layer in the upper soil decrease with time increases, which suggests that the anisotropy of the soil increases due to the crack propagation. However, we can also see that the measured AIs of some electrode layers keep increasing during the desiccation process, such as 0 mm in Fig.7a and 30 mm in Fig.7b. The occurrence of these two phenomena shows that the cracks are propagating in the soil, but the different directions of cracks cause this phenomenon. In the case of the electrode array arrangement in this study (Fig. 3), when the crack direction is the y direction, the increase of the crack depth will reduce the AI, and when the crack direction is the x direction, the increase of the crack depth will increase the AI. In the study of soil surface cracks, we found that most of the primary cracks and secondary cracks intersect perpendicularly, which will make AI change differently. However, the depth of the primary crack is generally much greater than that of the secondary crack. We can use this property to judge the propagation of the primary cracks and secondary cracks in

the soil. The anisotropy of soil apparent resistivity is related to electric field and conductor properties. The formation of cracks causes directional dependence of the current flow, which makes AI promising for detecting cracks.

3.5 Exploring the method of detecting crack depth

The cracks in the soil are full of air which is not conductive, so the cracks in the soil can be regarded as insulators [38]. The AI of the soil is related to the electric field distribution and the properties of the soil. For a multi-layer electrode array in the soil, the propagation of cracks will affect the AI measured by each electrode plane array. Predictably, the AI measured by the electrode plane array closest to the leading edge of the crack is most affected. For a multi-layer electrode array, when the leading edge of the crack passes through an electrode plane array (Fig. 8), the change of AI (ΔAI) measured by it should be the largest among all electrode plane arrays. We make a following assumption: in the process of using a multi-layer electrode array to measure ΔAI, if the ΔAI of a certain electrode plane array is the largest, indicating that the crack is near this electrode plane array.

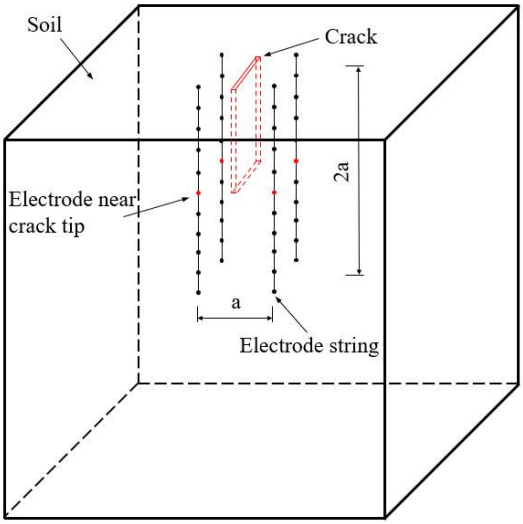

Fig 8: Schematic diagram of multi-layer electrode measuring single fissure

In order to verify the correctness of the above assumption, we build a numerical model as shown in Fig. 8. A total of 11 layers of electrode arrays are arranged, the spacing of each layer of electrode arrays is 0.2a, and a is the side length of the planar square electrode array. The width of the crack is set to 0.05a, and the length is a. Measuring the AIs of each layer of electrode array when the crack depths are 0.6a, 0.7a, 0.9a, 1.0, 1.6a, 1.7a, 1.8a and 1.9a, respectively. The eight crack depths are divided into four groups, and the AI of each group is subtracted to obtain the ΔAI. Fig. 9 shows the ΔAI of each electrode array layer corresponding to the combination of different crack depths.

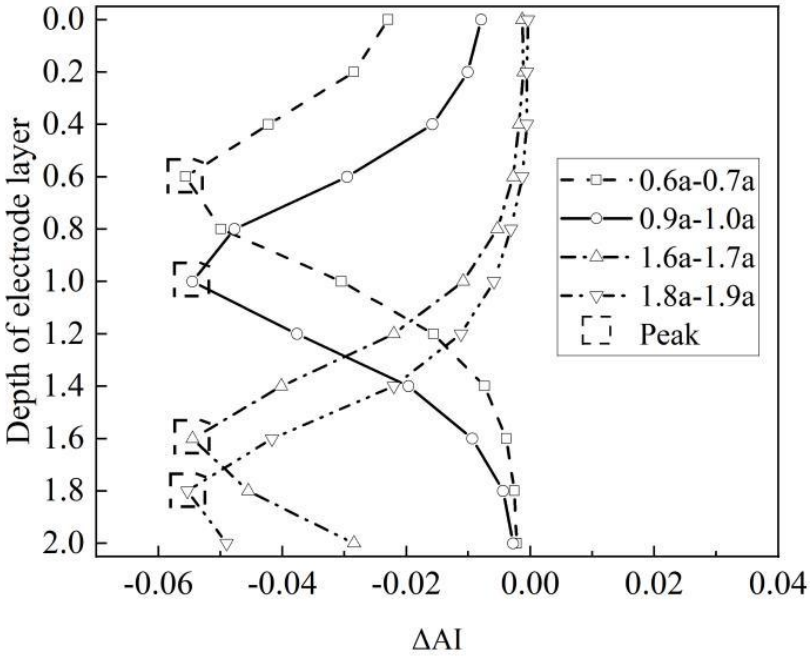

Fig 9: ΔAI distributions of numerical simulation at different measurement times

According to the above analysis, the crack direction in the numerical model is the y direction. As the crack depth increases, AI should continue to decrease, that is, ΔAI is negative, which is shown in Fig. 9. The peak of each group of ΔAI is approximately equal to the depth of its corresponding crack combination in Fig. 9. Because the distance between the electrode array layers is 0.2a, the error of the predicted depth could be 0.1a. We can see that the error of the predicted depth is less than 0.1a. Therefore, we might think that AI could be used to measure the crack depth. In order to verify the applicability of this method in actual fracture depth measurement, taking the AI measured by I and III cells as an example, each cell can get four groups of ΔAI after subtraction of two adjacent measurements of AI. The results are shown in Fig. 10.

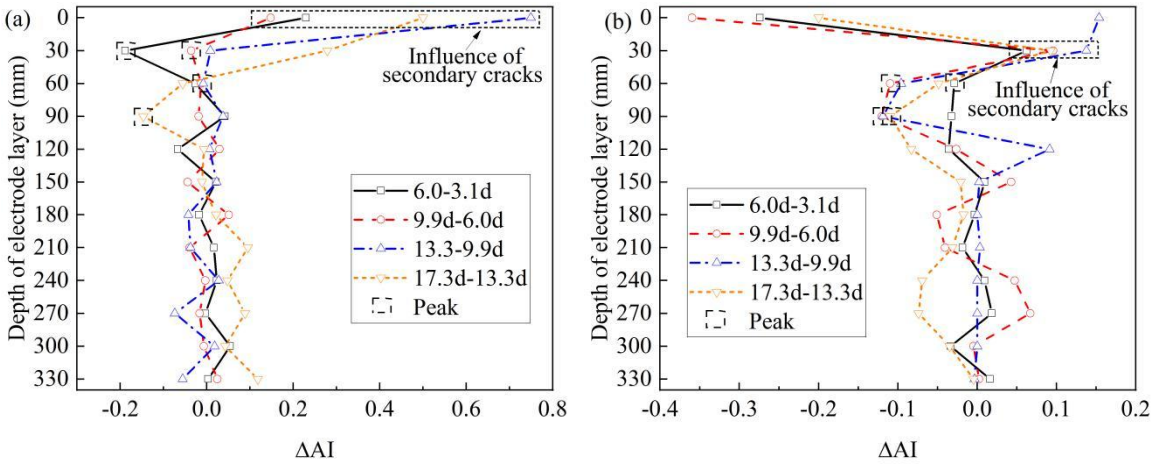

Fig 10: ΔAI distributions at different measurement times: (a) cell I, (b) cell III

In Fig. 10, some peaks are existed in each set of ΔAI data. Based on the above conclusions, the electrode burial depth corresponding to the ΔAI peak is the crack depth at this point. However, multiple peaks are present in some sets of ΔAI data, it should be caused by the propagation of secondary cracks. Because the depth of the primary crack is deeper than that of the secondary crack, the maximum depth corresponding to peak is the primary crack depth. For the electrode array in this study, if the directions of secondary cracks are perpendicular to the primary

crack, the AI will increase with the deepening of the secondary crack depth. As shown in Fig. 10a, AI at the electrode burial depth of 0 mm increases as the desiccation progresses. In Fig. 10b, AI at the electrode burial depth of 30 mm also increases as the desiccation progresses. For a certain electrode array, the primary cracks and secondary cracks have different effects on AI, which will cause different peaks of ΔAI. The depth of the primary crack is much greater than that of the secondary crack, and we only need to detect the maximum crack depth. Therefore, the burial depth of the electrode array corresponding to the deepest AI peak is roughly the largest crack depth.

3.6 Comparation of the AI method and the CTOA method

After the experiment, the soil model was excavated to obtain the CTOA of the soil [39]. Measure the width of the widest crack in each cell, and get the depth corresponding to the widest crack according to the excavation results (Table 2). Using Equation (6) can get the CTOA of the soil. The CTOA of the soil used in this experiment is about 2.99 °. Using AIs measured on day 3.1 and day 6.0 of the cell I as an example (Fig. 7a), the AIs measured in these two days were subtracted to get the ΔAI (Fig. 10a). From the aforementioned results, because the burial depth of the electrode corresponding to the ΔAI peak is 30 mm, we think the crack depth is 30mm on the 6th day. At this time, it is necessary to measure the widest surface crack width on the 6th day and to get the crack depth according to CTOA of 3°. The crack depth predicted by the ΔAI peak in cell I and cell III at different times and the crack depth obtained by CTOA are plotted in Fig. 11 to verify the effectiveness of this new method in detecting the soil crack depth. It can be seen that the depth obtained by the two methods is almost the same. The differences of crack depths obtained by the two methods are less than the allowable error, which is 0.5 times the electrode spacing (15 mm). Based on the above analysis, it can be considered that the method of detecting crack depth is useful.

Table 2 Results of soil excavation after the experiment

Cell	Ⅰ	Ⅱ	Ⅲ	Ⅳ
Maximum crack width (mm)	5.92	4.04	6.63	3.27
Maximum crack depth (mm)	103.86	85.94	109.4	75.00
CTOA (°)	3.27	2.70	3.48	2.50
CTOA mean (°)	2.99			

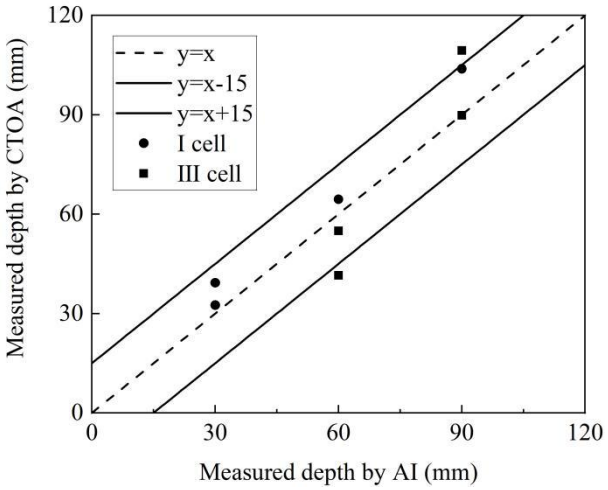

Fig 11: Depth comparison of AI prediction and CTOA prediction

3.7 Implication

This method could be used to detect crack depth of impermeable clay liner in landfill cover. When constructing the landfill cover, the electrode strings are arranged to form some multi-layer square electrode arrays in some positions of the clay liner that need to be monitored. During the service period of the landfill cover, an appropriate time interval can be selected to measure AIs. If AIs of different depths are not largely unchanged in different measurements, it indicates that there are no cracks in the clay liner and its sealing performance is good. If the distributions of AIs along the burial depth are different at different measuring moments, it indicates that cracks have occurred. By subtracting the AIs distribution sequences of two adjacent measurements, the burial depth of the electrode plane corresponding to the largest AI change (ΔAI) can be obtained. From the above analysis, it can be considered that the burial depth of the electrode plane corresponding to the ΔAI peak is the approximate depth of the crack. In order to ensure the accuracy of the measurement, the appropriate electrode layer spacing and measurement time interval should be selected. Too large electrode layer spacing will make the measurement error of the crack depth larger. If the crack develops quickly and the measurement time interval is too long, the electrode burial depth corresponding to the AI peak will be smaller than the actual crack depth.

IV. Conclusions

In this study, a desiccation experiment was performed to monitor soil crack in the laboratory, and the morphology of soil cracks during desiccation was analyzed. The changes of suction, water content and anisotropy index (AI) of apparent electrical resistivity during the crack propagation are studied. The ΔAI could be used to detect the soil crack depth. The major conclusions are as follows：

(1) The volumetric moisture content sensors and suction sensors are used to study the moisture migration in the process of soil desiccation, and it is found that cracks gradually expand with the decrease of water content and the increase of matric suction. During the desiccation process, since the water of the soil surface evaporates quickly, cracks appear on the surface of the soil first. During the evaporation process, the water content and suction of the soil in the horizontal and vertical directions are different, which causes uniform shrinkage of the soil. This is the reason for the desiccation cracks in the soil. During the desiccation process, the expansion of soil surface cracks was recorded by a camera, which verified the previous summary of soil surface crack morphology.

(2) This paper proposes a method for detecting the crack depth based on the anisotropy index (AI) of apparent electrical resistivity. For a multi-layer electrode array, when the leading edge of the crack passes through an electrode plane array, it has the greatest effect on the AI measured by the electrode plane array, which has been proved by a numerical simulation of a multi-layer electrode array in detecting the crack depth. Therefore, the crack depth can be detected by using the AI measured by a multi-layer electrode array, and the burial depth of the electrode plane array corresponding to the largest AI change (ΔAI) is the depth of the crack at this time. This method was compared with the CTOA method, which proved the effectiveness of this method in the measurement of crack depth. In order to make the measurement results more accurate, the distance between the electrodes should be selected appropriately, and the time interval between two adjacent measurements should not be too long. Using this method, the approximate crack depth can be obtained without inverting the measured apparent electrical resistivity. It is simpler than the electrical resistivity tomography method.

(3) In this paper, we use AI to detect the soil crack depth, and the experimental conditions are ideal. The actual soil crack measurement should be more complicated, which is specifically shown in the soil heterogeneity, complex crack networks, dry-wet cycle of soil. The duration of the laboratory experiment should be extended to further examine the applicability of AI in detecting the depth of natural cracks. In addition, the development of secondary cracks will also affect the AI. How to better distinguish the primary cracks and secondary cracks from the test results needs to be further researched. The applicability of this method for outdoor soil crack measurement needs to be further studied.

Acknowledgments

This article was funded by Natural Science Foundation Youth Project of China (Grant No. 41907252) and Guangdong Province Basic and Applied Basic Research Fund (Grant No. 2020A1515011398).

References

[1] Y.L. Gui, W. Hu, Z.Y. Zhao, et al., "Numerical modelling of a field soil desiccation test using a cohesive fracture model with Voronoi tessellations," Acta Geotechnica, vol. 13, no.1, pp. 87-102, 2018.

[2] T.D. Vo, A. Pouya, S. Hemmati, et al., "Modelling desiccation crack geometry evolution in clayey soils by analytical and numerical approaches," Canadian Geotechnical Journal, vol. 56, no.5, pp. 720-729, 2019.

[3] Q. Cheng, C.S. Tang, D. Xu, et al., "Water infiltration in a cracked soil considering effect of drying-wetting cycles," Journal of Hydrology, vol. 593, pp. 125640, 2021.

[4] D.P. Kanungo, R. Singh, R.K. Dash, "Field observations and lessons learnt from the 2018 landslide disasters in Idukki District, Kerala, India," Current Science, vol. 119, no.11, pp.1797-1806, 2020.

[5] E. Safari, M.J. Ghazizade, M.A. Abduli, et al., "Variation of crack intensity factor in three compacted clay liners exposed to annual cycle of atmospheric conditions with and without geotextile cover," Waste management, vol. 34, no.8, pp.1408-1415, 2014.

[6] F. Louati, H. Trabelsi, M. Jamei, et al., "Impact of wetting-drying cycles and cracks on the permeability of compacted clayey soil," European Journal of Environmental and Civil Engineering, vol. 25, no.4, pp. 696-721, 2021.

[7] C.S. Tang, D.Y. Wang, C. Zhu, et al., "Characterizing drying-induced clayey soil desiccation cracking process using electrical resistivity method," Applied Clay Science, vol.152, pp.101-112, 2018.

[8] D.Y. Wang, C.S. Tang, Y.J. Cui, et al., "Effects of wetting–drying cycles on soil strength profile of a silty clay in micro-penetrometer tests," Engineering Geology, vol. 206, pp. 60-70, 2016.

[9] J.H. Li, L. Li, R. Chen, et al., "Cracking and vertical preferential flow through landfill clay liners," Engineering Geology, vol. 206, pp: 33-41, 2016.

[10] M. Sánchez, O.L. Manzoli, L.J. Guimarães, "Modeling 3-D desiccation soil crack networks using a mesh fragmentation technique," Computers and Geotechnics, vol. 62, pp. 27-39, 2014.

[11] B. Velde, "Structure of surface cracks in soil and muds," Geoderma, vol. 93, no. 1-2, pp. 101-124, 1999.

[12] S.P. Singh, S. Rout, A. Tiwari, "Quantification of desiccation cracks using image analysis technique," International Journal of Geotechnical Engineering, vol. 12, no. 4, pp. 383-388, 2018.

[13] H.J. Vogel, "Morphological determination of pore connectivity as a function of pore size using serial sections," European Journal of Soil Science, vol. 48, no. 3, pp. 365-377, 1997.

[14] A. Besson, M. Seger, G. Giot, et al., "Identifying the characteristic scales of soil structural recovery after compaction from three in-field methods of monitoring," Geoderma, vol. 204, pp.130-139, 2013.

[15] A.S. Kishné, C.L.S. Morgan, W.L. Miller, "Vertisol crack extent associated with gilgai and soil moisture in the Texas Gulf Coast Prairie," Soil Science Society of America Journal, vol. 73, no. 4, pp. 1221-1230, 2009.

[16] M.R. Abou Najm, J.D. Jabro, W.M. Iversen, et al., "New method for the characterization of three‐dimensional preferential flow paths in the field," Water Resources Research, vol. 46, no.2, pp. W02503, 2010.

[17] M.E. Torbaghan, W. Li, N. Metje, et al., "Automated detection of cracks in roads using ground penetrating radar," Journal of Applied Geophysics, vol. 179, pp. 104118, 2020.

[18] K. Li, Z. Ma, P. Fu, et al., "Quantitative evaluation of surface crack depth with a scanning laser source based on particle swarm optimization-neural network," NDT & E International, vol. 98, pp. 208-214, 2018.

[19] J.P. Ackerson, K.J. McInnes, C.L.S. Morgan, et al., "Measuring Crack Porosity using Three‐Dimensional Electrical Resistivity Tomography," Soil Science Society of America Journal, vol. 81, no. 5, pp. 1025-1035, 2017.
[20] N. An, C.S. Tang, Q. Cheng, et al., "Application of electrical resistivity method in the characterization of 2D desiccation cracking process of clayey soil," Engineering Geology, vol. 265, pp. 105416, 2020.
[21] A. Samouëlian, I. Cousin, G. Richard, et al., "Electrical resistivity imaging for detecting soil cracking at the centimetric scale," Soil Science Society of America Journal, vol. 67, no. 5, pp. 1319-1326, 2003.
[22] A.K. Greve, R.I. Acworth, B.F. Kelly, "Detection of subsurface soil cracks by vertical anisotropy profiles of apparent electrical resistivity," Geophysics, vol. 75, no. 4, 85-93, 2010.
[23] A. Hassan, D.G. Toll, "Electrical resistivity tomography for characterizing cracking of soils," Geo-Congress 2013: Stability and Performance of Slopes and Embankments III, pp. 818-827, 2013.
[24] P. Qin, Y. Liu, Z. Song, et al., "An electrical resistivity method of characterizing hydromechanical and structural properties of compacted loess during constant rate of strain compression," Sensors, vol. 20, no. 17, pp. 4783-4798, 2020.
[25] T. Wen, P. Wang, L. Shao, et al., "Experimental investigations of soil shrinkage characteristics and their effects on the soil water characteristic curve," Engineering Geology, vol. 284, pp. 106035, 2021.
[26] Z. Huang, B. Wei, L. Zhang, et al., "Surface crack development rules and shear strength of compacted expansive soil due to dry–wet cycles," Geotechnical and Geological Engineering, vol. 37, no.4, 2647-2657, 2019.
[27] T. Zhou, P. Xin, L. Li, et al., "Effects of large macropores on soil evaporation in salt marshes," Journal of Hydrology, vol. 584, 124754, 2020.
[28] C.S. Tang, Y.J. Cui, A.M. Tang, et al., "Experiment evidence on the temperature dependence of desiccation cracking behavior of clayey soils," Engineering Geology, vol. 114(no. 3-4, pp. 261-266, 2010.
[29] M.N. Kulkarni, "On the modeling of electrical boundary layer (electrode layer) and derivation of atmospheric electrical profiles, eddy diffusion coefficient and scales of electrode layer," Journal of earth system science, vol. 119, no. 1, pp. 75-86, 2010.
[30] P. Areias, J. Reinoso, P.P. Camanho, et al., "Effective 2D and 3D crack propagation with local mesh refinement and the screened Poisson equation," Engineering Fracture Mechanics, vol. 189, pp. 339-360, 2018.
[31] X. Su, W.R. Tyson, B. Rothwell, "Recent developments in design for crack arrest using the cracktip opening angle (CTOA)," Journal of Pipeline Engineering, vol. 14, no. 4, pp. 241-247, 2015.
[32] M.T. Van Genuchten, "A closed‐form equation for predicting the hydraulic conductivity of unsaturated soils," Soil science society of America journal, vol. 44, no. 5, pp. 892-898, 1980.
[33] F.Q. Bai, S.H. Liu, "Measurement of the shear strength of an expansive soil by combining a filter paper method and direct shear tests," Geotechnical Testing Journal, vol. 35, no. 3, pp. 451-459, 2012.
[34] E. Romero, A. Gens, A. Lloret, "Water permeability, water retention and microstructure of unsaturated compacted Boom clay," Engineering Geology, vol. 54, no. 1-2, pp. 117-127, 1999.
[35] J.H. Li, Z. Lu, L.B. Guo, et al., "Experimental study on soil-water characteristic curve for silty clay with desiccation cracks," Engineering Geology, vol. 218, pp. 70-76, 2017.
[36] R.N. Tollenaar, L.A. Van Paassen, C. Jommi, "Observations on the desiccation and cracking of clay layers," Engineering geology, vol. 230, pp. 23-31, 2017.
[37] L.L. Wang, C.S. Tang, B. Shi, et al., "Nucleation and propagation mechanisms of soil desiccation cracks," Engineering Geology, vol. 238, pp. 27-35, 2018.
[38] T.A. Do, A.M. Lawrence, M. Tia, et al., "Effects of thermal conductivity of soil on temperature development and cracking in mass concrete footings," Journal of Testing and Evaluation, vol. 43, no. 5, pp. 1078-1090, 2015.
[39] K.V. Uday, D.N. Singh, "Investigation on cracking characteristics of fine-grained soils under varied environmental conditions," Drying Technology, vol. 31, no. 11, pp. 1255-1266, 2013.